Fast electron transport in laser-produced plasmas and the KALOS code for solution of the Vlasov–Fokker–Planck equation

2006 Plasma Phys. Control. Fusion 48 R37

(http://iopscience.iop.org/0741-3335/48/3/R01)

INSTITUTE OF PHYSICS PUBLISHING PLASMA PHYSICS AND CONTROLLED FUSION

Plasma Phys. Control. Fusion **48** (2006) R37–R57 doi:10.1088/0741-3335/48/3/R01

TOPICAL REVIEW

Fast electron transport in laser-produced plasmas and the KALOS code for solution of the Vlasov–Fokker–Planck equation

A R Bell[1], A P L Robinson[1,2], M Sherlock[1,2], R J Kingham[1] and W Rozmus[1,3]

[1] Imperial College, London, SW7 2AZ, UK
[2] Central Laser Facility, CCLRC, Chilton, Didcot, Oxfordshire, OX11 0QX, UK
[3] Department of Physics, University of Alberta, Edmonton, Canada

Received 31 August 2005, in final form 27 January 2006
Published 24 February 2006
Online at stacks.iop.org/PPCF/48/R37

Abstract

In solid targets irradiated by short pulse high intensity lasers, fast electrons have collision times longer than the laser pulse duration and mean free paths much larger than the radius of the laser spot. In these conditions, fast electron transport is dominated by electric and magnetic field. Although the fast electrons are collisionless, collisions of background electrons determine the ability of the background plasma to carry the return current which balances the fast electron current. Hence collisions are important even in this regime. A successful numerical simulation has to be able to model a plasma in which some electrons are collisionless and others are strongly collisional. An expansion of the electron distribution in spherical harmonics in momentum space is well suited to this, and we describe the formulation of the Vlasov–Fokker–Planck equation in terms of spherical harmonics and its solution in our KALOS code. We review the physics that must be modelled in a numerical simulation of fast electron transport and then describe KALOS.

1. Introduction

At laser intensities relevant to conventional inertial confinement fusion (ICF), energy is transported into the target mainly by thermal electrons. Some higher energy electrons (known as 'fast electrons') are produced by the absorption process, and the long-range preheat they cause can be important, but their overall contribution to energy transport is relatively small. The transport of fast electrons into a solid target at ICF laser intensities is dominated by collisions. In contrast, at the high intensities, 10^{16}–10^{20} W cm^{-2}, characteristic of short pulse high power lasers, most of the energy is transported by fast electrons which are almost collisionless. Their number and energy densities are large, and the electrical currents they carry produce large electric and magnetic fields which in turn affect the fast electron trajectories, notably limiting

their penetration into the target and collimating fast electrons into beams or filaments. Charge neutrality requires that a flux of fast electrons into the target must be balanced by a return current of thermal electrons which are collisional. This paper outlines the main features of field-dominated transport and demonstrates the need for a phase–space simulation code which encompasses both collisionless and strongly collisional electrons in one numerical model. Our KALOS code (Kinetic Laser-plasma Simulation) has been developed for this purpose. The unique feature of KALOS is that it expands the electron velocity distribution in spherical harmonics. Results from KALOS simulations have been presented previously [1–3], but this is the first time that the mathematical formulation underlying the code has been described. The earlier sections of this paper review the physics of fast electron transport and the thinking that went into the choice of the KALOS formulation of the Vlasov–Fokker–Planck (VFP) equation. We do not give specific difference equations since there are many ways that the KALOS equations can be differenced in keeping with the mathematical formulation in terms of spherical harmonics. Much of the content of section 2, describing the physics, has been published elsewhere, particularly in our own previous papers, but we find it helpful to collect it together here where we can supplement it with further analysis and comment. A related discussion by Davies can be found in [4].

2. The physics of fast electrons

2.1. Key quantities and relationships

Laser beams are unable to penetrate a plasma at solid density. Laser energy is partly reflected and partly transferred to electrons which then propagate away from the absorption region into the solid. Energy conservation requires that the energy flux carried by the heated electrons is approximately equal to the absorbed flux of laser energy. If the electrons (with density n_e) are heated to a temperature T (in eV) and escape the absorption region at their thermal velocity $(eT/m_e)^{1/2}$, they transport energy with a flux, $1.5n_eeT(eT/m_e)^{1/2}$, where it is assumed that the electrons have a Maxwellian velocity distribution. In practice, the electrons escape at a fraction of their thermal velocity; the fast electron distribution need not be Maxwellian, and, particularly, at high laser intensity, only a fraction of the electrons in the absorption region are heated and transport energy out of the absorption region. To account for these factors, the energy flux is usually written as $Q = fn_eeT(eT/m_e)^{1/2}$, or equivalently as $Q = fQ_{\text{free}}$, where $Q_{\text{free}} = n_eeT(eT/m_e)^{1/2}$ [5]. Q_{free} is commonly known as the 'free-streaming heat flow' and f as the 'flux limiter'. Transport at ICF laser intensities is non-local [6, 7], but the use of a flux limiter in fluid simulations provides an adequate means of modelling most experiments. Equating the absorbed laser energy flux to the electron energy fluxes gives

$$\eta I_{18} = 0.02 f n_{23} T_{\text{keV}}^{3/2}, \tag{1}$$

where T_{keV} is the energy of the energy-carrying electrons in keV, n_{23} is the density of energy carrying electrons in units of 10^{23} cm^{-3}, I_{18} is the laser intensity in units of 10^{18} W cm^{-2}, f is the flux limiter as defined above and η is the fraction of laser energy absorbed.

At intensities relevant to directly driven ICF, laser energy is absorbed by inverse bremsstrahlung close to the critical surface and raises the temperature of all electrons in an approximately Maxwellian thermal plasma. In this case, the density is fixed, the flux limiter is around 0.1 [6], the absorption is high and equation (1) determines the temperature of the plasma:

$$T_{\text{keV}} = 0.4\eta_{0.5}^{2/3} f_{0.1}^{-2/3} n_{22}^{-2/3} I_{14}^{2/3}, \tag{2}$$

where the same convention for units is used as above, e.g. I_{14} is the laser intensity in units of $10^{14}\,\mathrm{W\,cm^{-2}}$ and $f_{0.1}$ is f in units of 0.1 (i.e. $f_{0.1} = 1$ if $f = 0.1$). This notation convention will be used throughout this paper.

At higher laser intensities, the temperatures are higher and the plasma is less collisional. Consequently, the absorption process is collisionless and there is no reason why the absorbing plasma and the energy-carrying electrons should be Maxwellian. Instead, the energy is given to a small fraction of 'hot' or 'fast' electrons with a characteristic energy determined by the mechanics of the absorption process. In long pulse experiments, a substantial low density plasma corona is formed by ablation with a scalelength much longer than the laser wavelength. Collisionless absorption takes place by resonance absorption at the critical surface whereby large amplitude electron plasma waves, damped by wave breaking, are resonantly excited by the laser electromagnetic wave. In experiments with short laser pulses (<1 psec) without a pre-pulse, there is insufficient time for the development of a corona with a well-defined critical surface and the energy is absorbed by the laser fields pulling electrons out of the plasma into the vacuum and then returning them with high energy [8,9]. If absorption is collisionless, the energy of the heated electrons is determined by the mechanics of absorption, and equation (1) gives the number density of these fast electrons needed to carry the absorbed energy flux.

In short pulse experiments, a commonly used expression for the energy of the hot electrons is 'Beg's law' [10] derived from experiments with laser intensities in the range $10^{16}\,\mathrm{W\,cm^{-2}}$ to $5 \times 10^{18}\,\mathrm{W\,cm^{-2}}$:

$$T_{\mathrm{keV}} = 200(I_{18}\lambda_{\mu\mathrm{m}}^2)^{1/3}, \tag{3}$$

where the laser wavelength dependence is inserted to scale the result to wavelengths other than the $1.053\,\mu$m used in the experiment. Rearranging equation (1) gives

$$n_{21} = \frac{2\eta}{f} I_{18}(I_{18}\lambda_{\mu\mathrm{m}}^2)^{-1/2}. \tag{4}$$

At these high intensities $2\eta/f$ can be expected to be about one if the fast electrons freely escape the absorption region. Equation (4) shows that the density of fast electrons required to carry the energy flux can exceed the critical density, $1.1 \times 10^{21}\lambda_{\mu\mathrm{m}}^{-2}\,\mathrm{cm^{-3}}$. The fast electron density can be a substantial fraction of solid density if the fast electrons are confined near the target surface, with the implication that they are not always a small perturbation upon the electron distribution. Furthermore, the high fast electron energy and density imply a high pressure,

$$P_{\mathrm{Mbar}} = 640\frac{\eta}{f} I_{18}(I_{18}\lambda_{\mu\mathrm{m}}^2)^{-1/6} \tag{5}$$

and a correspondingly high energy density.

The large fast electron density implies a significant charge density and also a large current density and a large total current carried by fast electrons as they propagate into the target. As with equation (1), these can be derived from energy flux conservation giving

$$j_{16} = \eta I_{18} T_{\mathrm{MeV}}^{-1}; \qquad \mathcal{I}_{\mathrm{MA}} = 100\eta P_{100} T_{\mathrm{MeV}}^{-1}, \tag{6}$$

where j_{16} is the current density in $10^{16}\,\mathrm{Am^{-2}}$, $\mathcal{I}_{\mathrm{MA}}$ is the total current in megaamperes and P_{100} is the laser power in units of 100 TW. Using Beg's law for the fast electron energy, this becomes

$$j_{16} = 5\eta I_{18}(I_{18}\lambda_{\mu\mathrm{m}}^2)^{-1/3}; \qquad \mathcal{I}_{MA} = 500\eta P_{100}(I_{18}\lambda_{\mu\mathrm{m}}^2)^{-1/3}. \tag{7}$$

A fast electric current of the order of 100 MA through an area of the order of $100\,\mu\mathrm{m}^2$ is remarkable.

2.2. Collision times and lengths

The scattering mean free path of a fast electron with an energy given by Beg's law is

$$\text{mfp} = 10^4 Z^{-1} n_{23}^{-1} (I_{18}\lambda_{\mu\text{m}}^2)^{2/3} \mu\text{m} \tag{8}$$

and the corresponding collisional scattering time is

$$\tau_{\text{scatter}} = 60 Z^{-1} n_{23}^{-1} (I_{18}\lambda_{\mu\text{m}}^2)^{1/2} \text{ psec}, \tag{9}$$

where the collision time is taken from the NRL Plasma Formulary [11] with an extra factor of Z included to account for scattering by ions with $Z > 1$ and the Coulomb logarithm has been set to 5. The energy loss time is about Z times longer than the angular scattering time. The mean free path is much greater than the target size and the collision time is much greater than the duration of the laser pulse. At first sight this suggests that collisions should be unimportant for fast electron transport, at least during the laser pulse. Indeed the collisions have no effect on the fast electrons directly, but in fact the collisionality of the thermal electrons plays a vital role.

2.3. Electric field and transport inhibition

Suppose for a moment that the fast electrons enter the target without a balancing return current of thermal electrons. From Maxwell's equation $\partial E/\partial t = -j/\epsilon_0$, during a laser pulse lasting τ_{psec} psec the electric field increases to $6 \times 10^{15} \eta \tau_{\text{psec}} I_{18} (I_{18}\lambda_{\mu\text{m}}^2)^{-1/3}$ which would be sufficient to stop megaelectronvolt fast electrons in a distance of less than 1 nm. Clearly the electric field must draw a return current of thermal electrons into the absorption region to balance the escape of fast electrons. If we assume that the thermal electrons can be treated as a separate component of the plasma with a conventional electrical conductivity σ, then the return current, equal in magnitude and opposite in sign to the fast electron current j, is drawn by an electric field of magnitude $E = j/\sigma$, giving

$$E_{10} = 5\sigma_6^{-1} \eta I_{18} (I_{18}\lambda_{\mu\text{m}}^2)^{-1/3}, \tag{10}$$

where E_{10} is the electric field in units of $10^{10}\,\text{V m}^{-1}$ and σ_6 is the electrical conductivity in units of $10^6\,\Omega^{-1}\,\text{m}^{-1}$ which is approximately the conductivity of aluminium at 100 eV [12]. This electric field is sufficient to stop the fast electrons, with an energy following Beg's law, in a distance

$$L_{\mu\text{m}} = 4\sigma_6 \eta^{-1} I_{18}^{-1} (I_{18}\lambda_{\mu\text{m}}^2)^{2/3}. \tag{11}$$

Hence, the electric field required to draw the return current has about the right magnitude to inhibit the escape of fast electrons from the absorption region. The containment distance L is only weakly dependent on the laser intensity, but it has a strong dependence on the thermal plasma conductivity which can vary greatly with material and with temperature. Experiments on insulating targets could demonstrate severe transport inhibition due to electric fields provided the target remains cold so that the material, rather than the plasma, conductivity applies. There are a number of experiments in which electric field may be inhibiting fast electron transport (e.g. [13–16]; references to earlier experiments can be found in [17]). The importance of this effect has also been demonstrated by Guerin *et al* [18] who use a particle in cell (PIC) simulation with collisions to show that the fast electron transport is inhibited when collisions are turned on so that the thermal electrons are less able to provide a return current. If collisions are turned off, the mobile thermal electrons easily balance the fast electron current, the electric field remains small and the fast electron penetration is uninhibited.

A simple equation for the transport of fast electrons can be derived on the basis that (i) the fast electron current, $\boldsymbol{j}_f$, is balanced by a return thermal current, $\boldsymbol{j}_t$, $\boldsymbol{j}_f = -\boldsymbol{j}_t$, (ii) the electric

field drawing the return current is determined by the conductivity of the thermal plasma, $\boldsymbol{E} = \boldsymbol{j}_t/\sigma$, (iii) the fast electrons must obey the continuity equation for their number density, n_f, $\partial n_f/\partial t = \nabla \cdot (\boldsymbol{j}_f/e)$ and (iv) the electric field produces a potential ϕ which contains the fast electrons, giving $n_f \propto \exp(\phi/T)$ and $E = -(T/n_f)\nabla n_f$ where T is the fast electron temperature. Putting these equations together [17] gives

$$\frac{\partial n_f}{\partial t} = \nabla \cdot \left(\frac{\sigma T}{e n_f} \nabla n_f \right). \tag{12}$$

This has the form of a diffusion equation, but the diffusion coefficient, $D = \sigma T/e n_f$, is inversely proportional to fast electron density.

This diffusion equation can be solved analytically for special cases. If the number of fast electrons increases linearly with time as expected for constant laser irradiation, and the configuration is one-dimensional (in z), the equation has the solution [17]

$$n_f = n_0 \left(\frac{t}{t_{\text{laser}}} \right) \left(\frac{z_0}{z + z_0} \right)^2, \tag{13}$$

where τ_{laser} is a notional laser pulse duration and

$$n_0 = \frac{2\eta^2 I^2 \tau_{\text{laser}}}{9eT^3\sigma} \qquad \text{and} \qquad z_0 = \frac{3T^2\sigma}{\eta I}, \tag{14}$$

which, with Beg's law, is equivalent to

$$n_0 = \eta^2 \sigma_6^{-1} \tau_{\text{psec}} I_{18}^2 (I_{18}\lambda_{\mu\text{m}}^2)^{-1} 1.7 \times 10^{22}\,\text{cm}^{-3} \qquad \text{and}$$
$$z_0 = \sigma_6 \eta^{-1} I_{18}^{-1} (I_{18}\lambda_{\mu\text{m}}^2)^{2/3} 12\,\mu\text{m}. \tag{15}$$

Not surprisingly, z_0 has a magnitude and form close to that of $L_{\mu\text{m}}$ as calculated above, but it may be surprising that the penetration z_0 does not increase with time. The spatial form of the distribution remains constant, but the number density increases.

2.4. Ohmic heating of the thermal plasma

At high laser intensity, the energy loss time of fast electrons is longer than 1 psec, so the thermal plasma is only slowly heated by direct collisional energy transfer from fast electrons. In the same way that the electric field can dominate spatial transport, the electric field can also dominate energy exchange. The fast electrons lose energy as their electrical current does work against the electric field, and, correspondingly, the thermal electrons are ohmically heated with a volume heating rate $1.5 n_t e(\mathrm{d}\theta/\mathrm{d}t) = j_f^2/\sigma$, where θ is the thermal electron temperature in electronvolts and n_t is thermal electron density (see also [4]). Using equation (7) for the fast electron current density, the thermal electrons are heated during the laser pulse to a temperature $\theta = \sigma_6^{-1} n_{t,23}^{-1} t_{\text{psec}} \eta^2 I_{18}^2 (I_{18}\lambda_{\mu\text{m}}^2)^{-2/3} 90\,\text{keV}$. However, the plasma conductivity increases strongly with temperature so it is incorrect to set σ as a constant. The NRL Plasma Formulary [11], with the addition of the Z dependence and $\ln\Lambda = 5$ as above, gives the Spitzer plasma conductivity as $\sigma = 1.3 \times 10^8 Z^{-1} \theta_{\text{keV}}^{3/2}$. Integrating the heating equation, $1.5 n_t e\,\mathrm{d}\theta/\mathrm{d}t = j_f^2/\sigma$, with this expression for σ gives a time dependence for the thermal electron temperature and the conductivity,

$$\theta(t) = 1.3 n_{t,23}^{-2/5} t_{\text{psec}}^{2/5} Z^{2/5} \eta^{4/5} I_{18}^{4/5} (I_{18}\lambda_{\mu\text{m}}^2)^{-4/15}\,\text{keV}, \tag{16}$$

$$\sigma(t) = n_{t,23}^{-3/5} t_{\text{psec}}^{3/5} Z^{-2/5} \eta^{6/5} I_{18}^{6/5} (I_{18}\lambda_{\mu\text{m}}^2)^{-2/5} 2 \times 10^8\,\Omega^{-1}\,\text{m}^{-1}. \tag{17}$$

For intensities around $10^{18}\,\text{W cm}^{-2}$, the temperature rises to the order of 1 keV during the laser pulse, thus raising the conductivity and reducing the electric field to a level at which electric

field inhibition does not occur. Indeed, if the conductivity given by equation (17) were to apply throughout the target, one would conclude that electric field inhibition is unimportant except at low laser intensities. However, the plasma temperature in advance of the fast electron front is much lower than that given by equation (16) and inhibition can occur. It is evident that electric field inhibition is a complex phenomenon depending strongly on material properties. It is most effective at high Z and in insulators, and at laser intensities which are not so high as to rapidly heat the target to a large depth.

For some applications, it is desirable that electric field inhibition should be ineffective and that fast electrons should be able to propagate freely into the target. This requires delivery of sufficient energy to the target that the thermal temperature rises into the kiloelectronvolt range for the target to become strongly conducting. This sets an upper limit, given by $\eta I\tau \sim 1.5 n_t e\theta D$ for a one dimensional system, on the depth D to which the plasma can be heated to a temperature θ, giving

$$D \sim \eta_{0.2} I_{18} \tau_{\mathrm{psec}} n_{t,23}^{-1} \theta_{\mathrm{keV}}^{-1} 80\,\mu\mathrm{m}. \tag{18}$$

At intensities of $10^{18}\,\mathrm{W\,cm^{-2}}$, this allows heating and fast electron penetration to a substantial depth, but penetration may be limited by energy considerations at lower laser intensities.

Whether or not the electric field is sufficient to inhibit fast electron transport, it causes Ohmic heating of the thermal plasma. Because the conductivity rises rapidly with temperature, Ohmic heating raises the temperature to a ceiling value above which the heating process becomes relatively ineffective. Under a wide range of conditions, the temperature of the thermal plasma can be expected to reach and saturate at a few kiloelectronvolts.

The derivation of equations (16) and (17) assumed that the Spitzer conductivity can be applied to the thermal electrons. As noted above, this can be incorrect at lower laser intensities because of material properties. It can also be incorrect at high laser intensity due to distortion of the electron distribution and the contribution of runaway electrons. The Spitzer conductivity applies when the electron drift velocity is much smaller than the thermal velocity of the electrons carrying the current since it is derived by linearizing the electron distribution function about a zeroth order Maxwellian. It is well known that the Spitzer thermal conductivity ceases to apply when the heat flux approaches the 'free-streaming' value, $Q_{\mathrm{free}} = n_t e\theta (e\theta/m_e)^{1/2}$. Similarly, the linear electrical conductivity ceases to apply when the current approaches the 'free-streaming' current, $j_{\mathrm{free}} = n_t e (e\theta/m_e)^{1/2} = 2\times 10^{17} n_{t,23}\theta_{\mathrm{keV}}^{1/2}\,\mathrm{Am^{-2}}$. By the arguments used above, the return current carried by thermal electrons exceeds j_{free} and non-linear effects become important if

$$\eta I_{18} (I_{18}\lambda_{\mu\mathrm{m}}^2)^{-1/3} > 4 n_{t,23}\theta_{\mathrm{keV}}^{1/2}. \tag{19}$$

When the current approaches the free-streaming value, the electrons on the high velocity tail of the thermal Maxwellian distribution begin to accelerate freely. Since the collision time is proportional to the cube of the velocity, these electrons are less collisional. The acceleration due to the electric field exceeds the deceleration due to the frictional drag, these electrons become even less collisional as their velocity increases and they become run-aways (e.g. [19]). When this happens, the Spitzer conductivity no longer applies, the electron thermal distribution is no longer Maxwellian and the return current is carried by run-away electrons which short out the electric field.

2.5. Magnetic field

Any magnetic field must be small in the essentially one-dimensional configuration in which the fast electron penetration depth is much smaller than the radius of the laser spot. In practice,

experiments at high laser intensity are not one-dimensional since the laser spot is typically only 10 μm across. In 1D, electric forces dictate that the return current must locally balance the fast electron current. In 3D, one could envisage the situation in which the return flux of thermal electrons into the laser spot does not locally balance the fast electron current and in which the return current follows a route different from that of the escaping fast electrons, thus producing a circulating current and a strong magnetic field. We can demonstrate that inductive effects require that even in the 3D case with a small laser spot, the return and fast electron currents must balance out locally, i.e. $\boldsymbol{j}_f = -\boldsymbol{j}_t$, to a good approximation at every point.

Suppose for example that the fast electron current enters the target normally to the surface uniformly in a cylinder of radius r_f, and that the thermal return current, j_t, similarly flows uniformly in a cylinder but with a slightly larger radius, $r_t = r_f + \Delta r$. Both carry the same current $\mathcal{I}$, but in opposite directions: $j_f = \mathcal{I}/\pi r_f^2$, $j_t = \mathcal{I}/\pi r_t^2$. The magnetic field is then

$$B = \frac{\mu_0 \mathcal{I}}{2\pi} \begin{cases} r(r_f^{-2} - r_t^{-2}) & \text{if } r < r_f, \\ r^{-1} - r r_t^{-2} & \text{if } r_f < r < r_t, \\ 0 & \text{if } r_t < r. \end{cases} \tag{20}$$

If $\Delta r \ll r_f$, the peak magnetic field is $\mu_0 \mathcal{I}(\Delta r/r_f)/\pi r_f$ and the magnetic energy per unit length of the cylinder is $\mu_0 \mathcal{I}^2(\Delta r/r_f)^2/4\pi$. If $r_f = 10\,\mu$m and $\mathcal{I} = 100$ MA, the maximum magnetic field is $4 \times 10^4(\Delta r/r_f)$ MG and the magnetic energy per length of cylinder is $10^3(\Delta r/r_f)^2$ J μm^{-1}. The magnetic energy cannot be greater than the absorbed laser energy, so Δr must be much less than r_f for typical experimental parameters, even if all the absorbed energy is transferred to magnetic energy. This illustrates how the return current cannot follow a path much different from the fast electron current and must locally balance the fast electron current, $\boldsymbol{j}_f \approx -\boldsymbol{j}_t$.

An equation for the source and evolution of the magnetic field can be developed as follows. The origin of the magnetic field is the curl of the electric field required to draw the return current, $\partial \boldsymbol{B}/\partial t = -\nabla \wedge (\boldsymbol{j}_t/\sigma)$. Since the laser pulse duration is much greater than the light transit time, L/c, where L is a characteristic scalelength, the displacement current can be neglected, giving $\nabla \wedge \boldsymbol{B} = \mu_0(\boldsymbol{j}_f + \boldsymbol{j}_t)$. Putting these two equations together gives the magnetic field equation [20],

$$\frac{\partial \boldsymbol{B}}{\partial t} = -\nabla \wedge \left(\frac{1}{\sigma \mu_0} \nabla \wedge \boldsymbol{B} \right) + \nabla \wedge \left(\frac{\boldsymbol{j}_f}{\sigma} \right). \tag{21}$$

The first term on the right-hand side represents the resistive diffusion of magnetic field with diffusion coefficient $1/\mu_0\sigma$. The second term on the right-hand side is a source of magnetic field driven by the fast electron current. If the thermal plasma conductivity, σ, takes a value around $10^8\ \Omega^{-1}\ \mathrm{m}^{-1}$, typical of a 1 keV plasma, the diffusion coefficient is $\sim 10^{-2}\ \mu\mathrm{m}^2\ \mathrm{psec}^{-1}$ showing that, for practical purposes, resistive diffusion is small in plasmas at kiloelectronvolt temperatures and the magnetic field equation reduces [21] to

$$\partial \boldsymbol{B}/\partial t = \nabla \wedge (\boldsymbol{j}_f/\sigma). \tag{22}$$

The neglect of diffusion reinforces the conclusion above that the thermal return current must locally balance the fast electron current, although it is their very small spatial separation, leaving a total current density $\boldsymbol{j}_f + \boldsymbol{j}_t$, that produces the magnetic field.

Equation (22) predicts a magnetic field of the order of

$$B \sim jt/L\sigma \sim j_{16} t_{\mathrm{psec}} L_{\mu\mathrm{m}}^{-1} \sigma_8^{-1}\ \mathrm{MG}, \tag{23}$$

where L is the scalelength for variation in the fast electron current or the conductivity. This magnetic field is relatively small compared with the fields approaching 1 GG found at the

target surface [22, 23]. However, the field is large enough to collimate fast electron transport through the target as shown below, and it may under some circumstances be able to inhibit transport. As with the electric field, the magnitude of the magnetic field depends strongly upon the conductivity, so its influence depends on the material and on the temperature to which it is heated.

The mechanism for magnetic field generation described here operates within the solid target and is distinct from mechanisms operating at the target surface [22–24]. It is also distinct from magnetic field generation arising from laser propagation through a plasma [25] and from the baroclinic source ($\partial \boldsymbol{B}/\partial t \propto \nabla n_e \wedge \nabla T$) which requires a density gradient [26]. The mechanism considered here requires collisions and in this respect differs from the Weibel instability in its usual form [27, 28], although both are driven by electron anisotropy. It is more closely related to the collisional form of the Weibel instability [29, 30].

2.6. Magnetic field and fast electron beaming

A number of experiments demonstrate that fast electrons can pass through a solid target as a beam [31–35]. Given the impulsive nature of fast electron acceleration at the target surface, it is likely that fast electrons are accelerated anisotropically, but this cannot account for the tightly collimated beams seen in some experiments. For example, Tatarakis et al [31] find that energy transported to the rear of a 140–250 μm-thick target can arrive at a spot which is smaller than the laser spot at the front surface. The magnetic field produced by the return current as described in section 2.5 can be responsible for collimation as shown by Davies *et al* [36], Bell and Kingham [1] and Honrubia *et al* [37]. The azimuthal magnetic field surrounding the beam acts to deflect fast electrons into the beam thereby further collimating the beam. Suppose the acceleration process produces the fast electrons in a velocity cone of half-angle $\phi_{1/2}$. The magnetic field surrounding the cone of fast electrons is sufficient to collimate them into a narrow beam if $R/r_g > \phi_{1/2}^2$ where R is the radius of the beam and r_g is the Larmor radius of the fast electrons in the magnetic field. If this condition is satisfied, the magnetic field bends the fast electron trajectory through an angle $\phi_{1/2}$ in a distance $R/\phi_{1/2}$. From equation (23), $B \sim \eta I t/RT\sigma$, and the condition for collimation is

$$\eta I > \frac{\phi_{1/2}^2 \sigma m_e T}{e\tau}\left(\frac{eT}{m_e}\right)^{1/2} \qquad \text{or, equivalently, } \eta I_{18} > 7.5\times 10^{-4}\phi_{1/2}^2\sigma_8 T_{\text{keV}}^{3/2}\tau_{\text{psec}}^{-1}. \quad (24)$$

Using Beg's law this becomes

$$\eta I_{18}(I_{18}\lambda_{\mu\text{m}})^{-1/3} > 2\phi_{1/2}^2\sigma_8\tau_{\text{psec}}^{-1}, \quad (25)$$

where, as noted above for the Spitzer conductivity, $\sigma_8 = 1.3Z^{-1}\theta_{\text{keV}}^{3/2}(\log\Lambda/5)^{-1}$. As with electric field inhibition, resistive magnetic collimation depends strongly on the conductivity, σ. It therefore depends on the material properties and on the temperature to which the thermal plasma is heated. If the laser intensity is too low, equations (24) and (25) will not be satisfied. If it is too high, the plasma may be heated such that the conductivity is too large for resistive magnetic field generation to be important. It appears that resistive magnetic collimation may be limited to a fairly narrow range of experimental parameters. Equations (24) and (25) show that the half-angle, $\phi_{1/2}$, of the fast electron distribution as produced by the acceleration process has a strong determining effect on the occurrence of resistive magnetic collimation. If the fast electrons are already reasonably well beamed by the acceleration process, then further magnetic field collimation is much more likely.

Gremillet *et al* [38] and Honda [39] have demonstrated that this process can cause fast electron beams to further divide into separate beams or filaments. This has been observed in experiments in which considerable difference has been found between targets of different resistivity [40, 41].

2.7. Magnetic field caused by variations in resistivity

The equation $\partial \boldsymbol{B}/\partial t = \nabla \wedge (\boldsymbol{j}_f/\sigma)$ shows that, even for a uniform fast electron current $\boldsymbol{j}_f$, the magnetic field can grow if the conductivity has a gradient perpendicular to $\boldsymbol{j}_f$ since then $\partial \boldsymbol{B}/\partial t = -\boldsymbol{j}_f \wedge \nabla(1/\sigma)$. The conductivity will be non-uniform in the target if it is constructed of layers of different materials, particularly if the Z of each layer is very different. Even if the target is made of the same material throughout, the conductivity can vary due to variation in temperature, since $\sigma \propto \theta^{3/2}$, or in its state of ionization.

Consider a target with high Z material buried as a layer underneath the target surface. Such a layer is often used as a transport diagnostic. The buried layer will have a conductivity, σ_{B}, much lower than the conductivity, σ_{A}, of the surrounding low Z material. If the fast electron current passes normally across the buried layer, $\nabla \wedge (\boldsymbol{j}_f/\sigma)$ will be zero, but, away from the target axis, there will probably be a non-zero angle ψ between $\boldsymbol{j}_f$ and the normal to the buried layer. $\nabla \wedge (\boldsymbol{j}_f/\sigma)$ will be large at the surface of the buried layer and the magnetic field will grow with an integrated flux

$$\Psi = \int B \, \mathrm{d}z = j_f t (\sigma_{\mathrm{B}}^{-1} - \sigma_{\mathrm{A}}^{-1}) \sin\psi \approx j_f t \sigma_{\mathrm{B}}^{-1} \sin\psi \tag{26}$$

at the layer surface as shown in [20]. The actual peak value of the magnetic field at the surface depends on the resistive diffusion of the magnetic field away from its delta function source. However, the effect of the magnetic field on fast electron transport is determined by the integrated flux, Ψ, rather than the peak field. Fast electron transport is affected if the Larmor radius of a fast electron in the field is smaller than the spatial spread of the field about the surface, i.e. if $\Psi > (m_e/e)(eT/m_e)^{1/2} = 2.4 \times 10^{-3} T_{\mathrm{MeV}}^{1/2}$ Tm $= 24 T_{\mathrm{MeV}}^{1/2}$ MG μm. The condition for transport to be affected is

$$j_f \tau \sin\psi > \frac{\sigma_{\mathrm{B}} m_e}{e}(eT/m_e)^{1/2} \quad \text{or, equivalently, } \eta I_{18}(I_{18}\lambda_{\mu\mathrm{m}}^2)^{-1/2} \sin\psi > 2\sigma_8 \tau_{\mathrm{psec}}^{-1}. \tag{27}$$

This condition needs careful interpretation since the interaction with the buried layer may be deep inside the target, so geometrical effects can be important. For example, the value of j_f may be affected by spreading of the fast electron beam, and the buried layer may be relatively unheated so the relevant conductivity might be that of the cold unheated high Z material. Further discussion can be found by Bell *et al* [20] of the conditions in which the magnetic field at the surface of high Z layers might inhibit fast electron transport. Koch *et al* [34] have experimentally diagnosed fast electron transport and list this as one possible contributory factor in the emission patterns they see from buried layers.

Another situation in which non-zero $\nabla \wedge (\boldsymbol{j}_f/\sigma)$ might generate a magnetic field is at the target surface, particularly at the front where there may be large currents of fast electrons escaping a small laser spot. Large gradients in both current and conductivity must occur at the interfaces between the vacuum, the hot low density corona, the hot high density surface of the solid and the unheated solid. Given the complicated way in which the conductivity varies between layers, it is not clear how the magnetic field will grow, and further investigation is required.

Table 1. Conditions for field effects.

Effect	Section	Condition
Inhibition by electric field over a distance L	2.3	$\eta I_{18}^{1/3}\sigma_6^{-1} > 4L_{\mu\mathrm{m}}^{-1}$
Non-linear conductivity and run-away electrons	2.4	$\eta I_{18}^{2/3} n_{t,23}^{-1}\theta_{\mathrm{keV}}^{-1/2} > 4$
Magnetic collimation	2.6	$\eta I_{18}^{2/3}\sigma_8^{-1}\tau_{\mathrm{psec}} > 2\phi_{1/2}^2$
Magnetic inhibition due to layer of low conductivity	2.7	$\eta I_{18}^{1/2}\sigma_8^{-1}\tau_{\mathrm{psec}} \sin\psi > 2$

2.8. The importance of the thermal plasma

Table 1 lists the conditions for the occurrence of transport effects considered in this section. For simplicity, we assume that the laser wavelength is equal to 1 μm ($\lambda_{\mu\mathrm{m}} = 1$). The condition for inhibition due to electric field is given in terms of σ_6 instead of σ_8 because the fast electrons are penetrating into cold plasma with a conductivity which is lower than that of the hot thermal plasma heated by the passage of fast electrons. Most of the effects listed in the table have similar thresholds, although electric field inhibition can occur at lower laser intensity if the target is an insulator.

Table 1 shows that the conductivity plays an important role in determining whether these effects are important. The dependence on conductivity is greater than that on laser intensity. At low temperatures, the large difference between insulators and conductors makes the electric field inhibition strongly dependent on material properties as discussed in section 2.3. For magnetic collimation and magnetic inhibition the conductivity at kiloelectronvolt temperatures is important, and this is strongly dependent on the Z of the material and the state of ionization, and so once again experimental results vary with material as discussed in section 2.6. Furthermore, when the return current becomes non-linear and the Spitzer conductivity ceases to apply (section 2.4), a kinetic description of thermal as well as fast electrons is needed if the return current and the effective non-linear conductivity are to be modelled correctly. These considerations make it clear that successful modelling of fast electron transport depends on accurate modelling of low velocity electrons at least as much as it does on the accurate modelling of the fast electrons themselves.

3. Computational models

3.1. Requirements for a successful model

The previous sections of this paper have outlined various ways in which electric and magnetic fields are generated by fast electrons and how they feed back on to fast electron transport. The back-of-the-envelope calculations presented above are illuminating but they are too limited to model experiments accurately or predict the behaviour of future experiments. This is particularly true when phenomena depend upon a delicate balance of conditions. For example, correct modelling of the conductivity is essential since this determines the electric field needed to draw the return current and the curl of the electric field determines the growth of the magnetic field.

We now examine the physics that a numerical simulation must include and show that the conditions of short-pulse high intensity experiments are such that new simulation techniques are desirable.

3.1.1. Phase-space modelling of collisionless fast electrons. The collision times of fast electrons exceed the laser pulse duration, and their collision mean free paths exceed the laser spot size and usually the target thickness. Collisions are too weak to make the fast electron

distribution Maxwellian and a viable numerical model must be able to model highly structured velocity distributions as shown by PIC simulations of fast electrons produced by collisionless absorption [9, 42, 43]. Moreover, fast electrons are produced anisotropically, and magnetic collimation as discussed above further increases the anisotropy. Consequently, any numerical model must calculate the electron distribution in phase space with high resolution in all three momentum directions.

3.1.2. Phase-space modelling of collisional thermal electrons. The transport of fast electrons is dominated by electric and magnetic fields arising from the return current of resistive thermal electrons. The thermal electron conductivity is determined by collisions. Hence, collisions form an essential part of any numerical model. The collisional scattering time of a 100 eV electron at solid density is of the order of 0.1 fsec. The fast electrons flow into an initially unheated plasma which is dominated by collisions. In the initial stages of an experiment, the unheated thermal electron population can be treated as a fluid with a conductivity. However, Ohmic heating soon raises the kinetic energy of the thermal electrons, particularly the more mobile electrons on the high velocity tail of the thermal distribution which contribute most to the electrical conductivity. Ohmic heating enlarges the high velocity tail to the distribution, and, as shown in section 2.4, the linear Spitzer conductivity fails to apply. Thermal electron run-away can occur and short out the electric field. These essential effects can only be properly modelled if the thermal as well as the fast electrons are modelled in phase space. Thermal collisional electrons are promoted into collisionless electrons by Ohmic heating, by run-away, and also by the absorption of laser energy since the thermal electrons provide the pool of electrons for acceleration as they are pulled to the target surface by the electric field. The thermal and fast electrons can be treated separately as different populations in some problems in which the thermal electrons are only weakly heated, but in most cases they should be treated as one single undivided population.

3.1.3. Material properties and ionization. Fast electrons initially propagate into a cold thermal plasma. The Spitzer conductivity only applies when the temperature increases to a few hundred electronvolts. At lower temperatures, the property of the material as an insulator or conductor determines the conductivity. For example, solid aluminium has a minimum conductivity at around 100 eV. Furthermore, the specific heat of the material determines how rapidly the temperature rises during Ohmic heating. Even after the target becomes a plasma, its state of ionization determines the number of free electrons available to carry the return current. Consequently, both the ionization process and the material properties before ionization are an important part of the problem. Both field and collisional ionization are important. It is found experimentally that results can vary strongly between targets constructed of different materials (e.g. [40,41]). Ionization has been included in a VFP code by Town *et al* [44], Ethier and Matte [45] and Robinson *et al* [2]. Davies *et al* [36] included material properties in their hybrid code.

3.1.4. Dynamic range. A large dynamic range between the maximum and minimum values of physical parameters makes large demands on computational resources. Dynamic ranges can be especially large in fast electron transport simulations because of the difference between the parameters of the fast and thermal electrons. The principal parameters have the following dynamic ranges:

(i) The range of electron energies must extend to many megaelectronvolts to encompass the high energy relativistic tail of the fast electron distribution. It must also model electrons

with energies as low as 100 eV to model the return current and preferably as low as a few electronvolts if ionization is to be modelled. Thus a dynamic range of the order of 10^6 in energy or 10^3 in momentum is needed.

(ii) The Debye length in a 100 eV plasma at a density of $10^{23}\,\mathrm{cm}^{-3}$ is $2 \times 10^{-4}\,\mu$m, and this rules out any simulation model that needs to resolve the Debye length over the full length of the computational grid. The Debye length of the more energetic low density fast electrons is typically around $0.1\,\mu$m, and this must be resolved if the target surface is to be modelled. This implies a factor of $\sim$1000 between the smallest scalelength and the target thickness.

(iii) The shortest timescales are collision times, ionization times and oscillation times in the laser field, each of which is of the order of 0.1 fsec. The factor of 10^4 between the shortest timescales and the laser pulse duration is not extreme. However, implicit algorithms are desirable because they can allow integration over the shortest timescales and concentration on the longer timescales over which the system evolves as a whole. If it were necessary to resolve the collision times of electrons at ionization energies and solid density, the number of timesteps would be restrictively large.

(iv) Absorbed energy of 100 J is sufficient to raise 6×10^{15} fast electrons to an energy of 100 keV. In comparison, a cube of dimension $100\,\mu$m of solid density plasma contains the much larger number of around 6×10^{17} thermal electrons. In a particle simulation with both thermal and fast electrons treated equally, the total number of particles simulated would be unmanageably large if the fast electrons were to be adequately modelled.

3.1.5. Maxwell's equations. The full Maxwell equations are needed if laser absorption is to be modelled. The evolution of the magnetic and electric fields is calculated from $\partial \boldsymbol{B}/\partial t = -\nabla \wedge \boldsymbol{E}$ and $\partial \boldsymbol{E}/\partial t = c^2 \nabla \wedge \boldsymbol{B} - \boldsymbol{j}/\epsilon_0$. The second of these equations can in principle be replaced by Gauss's flux law in a one-dimensional transport problem in which laser propagation can be neglected, but even in this case the computation is usually more robust if the electric field is calculated from $\partial \boldsymbol{E}/\partial t = -\boldsymbol{j}/\epsilon_0$. The two time-dependent Maxwell equations and the VFP equation are the controlling equations of kinetic plasma simulation. The role of the VFP equation is to provide a relationship between $\boldsymbol{j}$, $\boldsymbol{E}$ and $\boldsymbol{B}$ for inclusion in the Maxwell equations.

3.1.6. Dimensionality. Some problems are one-dimensional, notably those in which the laser spot can be considered to be very large. Electrical inhibition is one-dimensional when the confinement distance is smaller than the laser spot radius, and many aspects of the shielding process at the rear surface are one-dimensional since the shielding length is small compared with the laser spot radius. However, even experiments with thin targets are not purely one-dimensional since the lateral escape of fast electrons reduces the fast electron density and changes conditions in the laser spot. In order to achieve the highest possible laser intensities on target, the laser spot is often reduced to a very small radius and strong 2D effects are inevitable. Phenomena such as magnetic field generation and fast electron collimation are inherently two- or three-dimensional.

From symmetry, transport from a circular laser spot assumes a two-dimensional cylindrical geometry and the only non-zero component of the magnetic field is B_θ corresponding to currents in the r and z directions only. In any realistic model of the laser absorption process other components of $\boldsymbol{B}$ are also non-zero.

Except for a limited set of problems, simulations are at least two-dimensional in space and three-dimensional in momentum. This inherently five-dimensional problem with time

evolution is demanding in computational memory as well as execution time. Previous VFP codes in two spatial dimensions have reduced the computational requirements by retaining only the zeroth and first order spherical harmonics [46–48], but this is insufficient at high laser intensities when fast electron transport is important.

3.2. Simulation methods

Any simulation of high intensity laser–solid interactions must include a kinetic treatment of fast electrons. The various simulation methods can be classified as (i) PIC, (ii) Vlasov, (iii) VFP, (iv) hybrid fluid/particle and (v) gridless particle codes.

PIC has been the most widely used method for kinetic simulation of laser-produced plasmas. The method is elegant, robust and efficient. Its basic advantage is that it is very close to being a 'numerical experiment'. It makes fewer approximations than any of the other methods. That the particle density can never become negative makes the method robust. The disadvantages of PIC for high intensity experiments are that (i) collisions and ionization are not easily included when their characteristic timescales are very short, (ii) the number of particles is prohibitively high when the fast electrons constitute a small fraction of the total and the Debye length, which must be resolved, is small for thermal electrons and (iii) PIC does not include material properties. Collisions have successfully been included in PIC codes ([49] and references therein) when collision times are relatively long but other methods are needed when particles are highly collisional. PIC remains unsurpassed for highly non-linear collisionless processes, such as absorption. As laser intensities increase yet further, the generation of electric and magnetic fields may become so rapid that collisions, ionization and material effects are unimportant, but for the present the use of PIC is relatively limited at high plasma densities.

Vlasov codes ([50], and references therein) describe electrons in terms of their distribution function and this avoids the statistical problem of following fast electrons which are a small fraction of the total number of electrons. Vlasov codes do not have to spatially resolve a Debye length in all problems. Explicit Vlasov codes have to temporally resolve Langmuir oscillations, but this can be avoided by making the field calculation implicit. Vlasov codes are not as close to the physics as PIC codes, but they make relatively few approximations. The main difficulty with a standard Vlasov code is the number of phase space grid-points needed in two spatial dimensions. A reasonable number of Cartesian grid-points in each of x, y, p_x, p_y and p_z is resource-intensive in memory and computational time. Vlasov codes work well in 1D, especially when only one dimension is needed in momentum, but a full $2\frac{1}{2}$D Vlasov simulation is much less efficient than a comparable PIC code. A Cartesian grid in momentum space is poorly adapted to accurate modelling of processes, such as collisions and gyration in a magnetic field, which naturally move electrons diagonally across the momentum grid.

VFP codes are designed to work well in collision-dominated plasma. The diffusive ('$f_0 + f_1$') approximation [51–53], in which the distribution takes the form $f(\boldsymbol{p}, \boldsymbol{r}, t) = f_0(|\boldsymbol{p}|, \boldsymbol{r}, t) + \boldsymbol{p} \cdot \boldsymbol{f}_1(|\boldsymbol{p}|, \boldsymbol{r}, t)/|\boldsymbol{p}|$, has proved very effective for thermal transport. This expression for f uses the first two terms of a spherical harmonic expansion in which the nth term decays exponentially at a rate proportional to $n(n+1)/2$. The rapidly damped higher order terms can be neglected if the electrons are collisional, and the approximation works well when the plasma is reasonably isotropic for other reasons. The main non-local effects in thermal transport result from the deviation of f_0 from Maxwellian and this is well treated by the diffusive approximation. Because this approximation keeps limited information about the distribution function, it can be made implicit [52,53]. Implicit solution allows a large timestep,

but the matrix manipulations can be very complicated when magnetic field is included. The $f_0 + f_1$ approximation has many advantages for non-local thermal transport, but it cannot model the fast electron anisotropy at high laser intensities, particularly when beaming occurs. The approximation cannot model laser absorption. The original VFP code of Bell *et al* [6] kept higher order anisotropy by expanding in Legendre polynomials, and this method has been further developed by Matte and co-workers [54, 55], but a Legendre polynomial expansion only models fluxes in one dimension. VFP codes have the advantage that they can include ionization and material effects.

Hybrid codes have proved a very efficient simulation of targets dominated by fast electron transport. Using a PIC model for fast electrons coupled to a conducting, but stationary, fluid model of the thermal plasma, Davies *et al* [36] (see also [4, 37, 38, 56]) demonstrated that beaming at high laser intensities could be explained by resistive magnetic collimation. Hybrid codes execute rapidly and can easily include a conductivity which is dependent on material properties. The limitations of hybrid codes arise from the separation of electrons into two populations, the need to transfer electrons between the two populations and the assumptions made about the thermal population. The LSP code [57] is being extended to include an impressive range of physics. Because of its assumptions and approximations it is being validated against experiments and less approximate models. In many respects hybrid codes are a development of the fast electron transport packages that have served well in ICF codes such as LASNEX.

Gridless particle codes [58] are a relatively recent introduction to the simulation of laser-produced plasmas. Some advantages are that relatively little computational effort needs to be expended on the vacuum or computational boundaries and that it is possible to model binary large-angle collisions between individual particles. Gridless particle codes offer the most complete model of a plasma, but this can be at a large cost in computational resources.

Each of the above models operates well in particular regimes on particular problems. However, none of the above, except potentially the gridless particle model, are good for modelling the self-consistent interaction between absorption and transport, and none of them successfully models run-away electrons and other non-Maxwellian effects which require the electrons to be modelled as a single distribution including both collisionless anisotropic fast electrons and collision-dominated cold thermal electrons. In the next section, we define a simulation code, KALOS, which is capable of efficiently modelling all these effects. There are many problems in which PIC, Vlasov, VFP, hybrid or gridless particle codes are best, but KALOS is intended to reach problems that other codes cannot reach. It is also intended to work very well as a traditional Vlasov or VFP code if collisions are, respectively, very weak or very strong.

4. KALOS

4.1. The spherical harmonic expansion used in KALOS

KALOS is a multi-dimensional Vlasov code, with added collisions and ionization, in which the electron distribution function is represented in momentum space (p, θ, ϕ) by an expansion in spherical harmonics:

$$f(\boldsymbol{r}, \boldsymbol{p}, t) = \sum_{n=0}^{n_{\max}} \sum_{m=-n}^{n} f_n^m(\boldsymbol{r}, p, t) P_n^{|m|}(\cos\theta) \mathrm{e}^{\mathrm{i}m\phi} \qquad \text{where } f_n^{-m} = (f_n^m)^*. \tag{28}$$

4.1.1. Some advantages of spherical harmonics.

(i) The dominant collision process is angular scattering by ions which is approximately Z times faster than collisional changes in energy. Angular scattering operates separately on each spherical harmonic, making its amplitude decay exponentially at a rate proportional to $n(n+1)/2$. Computational implementation is simple and accurate. If collisions are strong, only very few terms are needed in the spherical harmonic expansion. Even if collisions are weak, the $n(n+1)/2$ dependence means that the highest n spherical harmonics are damped allowing a natural termination to the expansion.

(ii) Magnetic field rotates the direction but not the magnitude of momentum, so it connects only f_n^m at the same n, but different m, and does not require a differential operator in momentum space. Hence the effect of a magnetic field is easily and accurately represented.

(iii) The use of the magnitude of momentum as a coordinate makes it relatively easy to introduce material effects such as ionization and non-plasma effects in the cells close to the origin.

(iv) The use of the magnitude of momentum as a coordinate means that the momentum grid can be stretched at large momentum and compressed at low momentum to give resolution where it is needed without increasing the total number of grid-points excessively.

(v) Calculations usually require less resolution in angle (θ, ϕ) than in magnitude, p. This is true when collisions damp the high n harmonics as noted above, but it is also true in many collisionless problems since the initial distribution is usually isotropic and anisotropy takes time to develop. Also, sometimes, spatial advection and scattering by electric and magnetic fields can act to reduce anisotropy, although the reverse can be true and this has to be tested for each case. The number of effective data points in momentum space is $N_p = n_{\max}^2 n_p$ where n_p is the number of grid points in magnitude of momentum and $n_{\max}$ is the highest order of the spherical harmonic expansion. N_p is usually significantly smaller than the number of momentum grid-points needed on a 3D square momentum grid as conventionally used in Vlasov codes.

(vi) Although spherical harmonics appear to have a preferred axis in the $\theta = 0$ direction, they are in many respects a formulation which is direction-independent and calculations with KALOS confirm this. Certainly there is no preferred direction in ϕ. A conventional square-gridded Vlasov code responds well for electric fields solely in the x, y or z directions but copes less well with a more generally directed field which moves electrons diagonally across the grid. In KALOS the only partial derivative in momentum is in $|\boldsymbol{p}|$, and experience shows that KALOS copes well with an electric field in any direction.

(vii) Electron–electron collisions are calculated using a formalism based on the Rosenbluth potentials which are calculated by integration in momentum over f_n^m. If all terms are included, the collisional interaction of each component, $f_{n_1}^{m_1}$, of the electron distribution with every other component, $f_{n_2}^{m_2}$, would have to be calculated—a prohibitively large total of $n_{\max}^4$ interactions. However, if collisions play a significant role, the distribution of low energy electrons is nearly isotropic in the ion rest frame. Provided the collision term is implemented in the ion rest frame, it is sufficient to calculate the Rosenbluth potentials from only the first few spherical harmonics. For example, the main effect of electron–electron collisions on high energy electrons is their collisional energy loss to the relatively large number of nearly isotropic thermal electrons. If the ions are treated as immobile then momentum is not conserved overall and it is sufficient to consider collisions only with the isotropic (f_0^0) part of the electron distribution. If ion motion is included, momentum can be conserved by calculating the Rosenbluth potentials for, and including collisions with, the f_1^m part of the distribution. In either case, the electron–electron part of the collision

term is considerably simplified. This approximation is better for high Z plasmas since the dominant collisions are then with ions rather than electrons.

4.1.2. Some disadvantages of spherical harmonics.

(i) KALOS does not automatically maintain positivity. If the spherical harmonic expansion is truncated, it is possible for f to become negative.
(ii) The origin at $p = 0$ requires careful treatment since a strong electric field advects electrons rapidly across this point. To cope with this (a) the spherical harmonic expansion is truncated in the first few grid-points in momentum to avoid excessive and unbalanced angular resolution in comparison with the resolution in p and (b) the components of the distribution function f_n^m are expanded as a power series in small p close to $p = 0$.

These difficulties, (i) and (ii), are not found to cause significant problems individually. It is found that they can work together deleteriously at an abrupt collisionless plasma/vacuum interface, but one way to reduce the problem is by the addition of some backward de-centring of the time difference in the momentum calculation in the first few cells in p. If collisions are important, the high collision rate ($\propto p^{-3}$) close to $p = 0$ makes the distribution approximate to an isotropic Gaussian locally in momentum space and the solution is robust.

Expansion in spherical harmonics might appear complicated and prone to numerical difficulty, but in fact the equations turn out to be fairly straightforward, probably, as found in many branches of physics, because spherical harmonics are a natural basis for angular calculations in 3D.

4.2. The equations solved by KALOS

KALOS solves the Vlasov equations with a Fokker–Planck collision term in two spatial and three velocity dimensions. The $2\frac{1}{2}$D KALOS equations can be written in the form

$$\frac{\partial f_n^m}{\partial t} - \mathcal{C}_{n,i}^m - \mathcal{C}_{n,e}^m - \mathcal{B}_n^m = \mathcal{A}_{n,x}^m + \mathcal{A}_{n,y}^m + \mathcal{E}_{n,x}^m + \mathcal{E}_{n,y}^m + \mathcal{E}_{n,z}^m \tag{29}$$

for the evolution of all f_n^m except for the imaginary part of f_n^0 which must always be zero because of the condition $f_n^{-m} = (f_n^m)^*$. The terms on the right-hand side are normally treated explicitly, while those on the left are normally treated implicitly.

4.2.1. Collisional scattering by stationary ions.

$$\mathcal{C}_{n,i}^m = -\frac{n(n+1)}{2}\nu(p) f_n^m. \tag{30}$$

This term represents the exponential decay of each spherical harmonic for $n > 0$ due to collisional scattering by ions and other electrons. $\nu(p) \propto p^{-3}$ is the momentum-dependent collisional damping rate for $n = 1$ as given by Shkarofsky *et al* [59].

4.2.2. Collisions between electrons. $\mathcal{C}_{n,e}^m$ represents collisions between electrons. In its complete form it can be written in the form

$$\mathcal{C}_{n,\,e}^m = \sum_{n'} \sum_{m'} \mathcal{C}_{n,n',e}^{m,m'}, \tag{31}$$

where $\mathcal{C}_{n,n',e}^{m,m'}$ represents collisions with the part of the electron distribution function represented by the spherical harmonic with coefficient $f_{n'}^{m'}$. Each $\mathcal{C}_{n,n',e}^{m,m'}$ is a second order differential in momentum space including the Rosenbluth potentials which are integrals in momentum space

over $f_{n'}^{m'}$. If included in full, electron–electron collisions require a lengthy and time-consuming computation. As mentioned above, the dominant terms are

$$\mathcal{C}_{n,e}^{m} = \mathcal{C}_{n,0,e}^{m,0} + \mathcal{C}_{n,1,e}^{m,0} + \mathcal{C}_{n,1,e}^{m,1} \tag{32}$$

and in most cases, the first of these three terms is sufficient since usually the bulk of electrons are thermal and slowly drifting. In its present form, KALOS keeps only the first term, which means that electron–electron collisions do not conserve momentum. However, the momentum error is small compared with that due to momentum loss to ions which are assumed to be stationary and act as a momentum sink. The electron-ion collision term is larger than the electron-electron term by a factor Z. The electron–electron collision term is important for the slowing down of energetic electrons as they lose energy to low energy electrons.

In the approximation that $\mathcal{C}_{n,e}^{m} = \mathcal{C}_{n,0,e}^{m,0}$, $\mathcal{C}_{n,0,e}^{m,0}$ can be separated into two parts. The first part is angular scattering, and this is straightforwardly added to the electron–ion term, $\mathcal{C}_{n,i}^{m}$, by adding a modification of order $1/Z$ to $\nu(p)$. The other part is a second order differential in magnitude of momentum, representing energy transfer between electrons, which can be included implicitly with Chang–Cooper differencing [60].

4.2.3. Magnetic field. The rotation of the distribution function in three-dimensional momentum space by the magnetic field (B_x, B_y, B_z) is represented for $m > 0$ by

$$\mathcal{B}_{n}^{m} = -\mathrm{i}\frac{eB_x}{m_e} m f_n^m - \frac{1}{2}\frac{e}{m_e}[(n-m)(n+m+1)(B_z - \mathrm{i}B_y) f_n^{m+1} - (B_z + \mathrm{i}B_y) f_n^{m-1}]. \tag{33}$$

For $m = 0$,

$$\Re[\mathcal{B}_{n}^{0}] = -\frac{e}{m_e}\, n(n+1)(B_z \Re[f_n^1] + B_y \Im[f_n^1]) \tag{34}$$

where $\Re$ denotes the real part. Because each term of the equation has the same n and connects only f_n^{m-1}, f_n^m and f_n^{m+1}, this is an algebraic complex tri-diagonal matrix equation which can be solved by standard methods using a time-centred trapezium scheme to integrate implicitly in time.

The magnetic field itself is updated from the Maxwell equation $\partial \boldsymbol{B}/\partial t = -\nabla \wedge \boldsymbol{E}$.

4.2.4. Spatial advection. For all m ($m \geqslant 0$) the spatial advection term in x (the $\theta = 0$ direction) is given by

$$\mathcal{A}_{n,x}^{m} = -\left(\frac{n-m}{2n-1}\right) v\, \frac{\partial f_{n-1}^{m}}{\partial x} - \left(\frac{n+m+1}{2n+3}\right) v\, \frac{\partial f_{n+1}^{m}}{\partial x}. \tag{35}$$

In two spatial dimensions we need only advection in x and y, but the equations in y and z are very similar. For $m > 0$,

$$\mathcal{A}_{n,y}^{m} = -\frac{v}{2}\,\frac{1}{2n-1}\left[\frac{\partial f_{n-1}^{m-1}}{\partial y} - (n-m)(n-m-1)\frac{\partial f_{n-1}^{m+1}}{\partial y}\right] + \frac{v}{2}\,\frac{1}{2n+3}\left[\frac{\partial f_{n+1}^{m-1}}{\partial y} - (n+m+1)(n+m+2)\frac{\partial f_{n+1}^{m+1}}{\partial y}\right]. \tag{36}$$

For $m = 0$,

$$\Re\left[\mathcal{A}_{n,y}^{0}\right] = \Re\left[v\frac{n(n-1)}{2n-1}\frac{\partial f_{n-1}^{1}}{\partial y} - v\frac{(n+1)(n+2)}{2n+3}\frac{\partial f_{n+1}^{1}}{\partial y}\right].$$

Apart from the coefficients in n and m, these are fairly standard advection equations which can be solved in a number of different ways. We find that a simple second order Runge–Kutta

scheme gives good results, although we have successfully implemented a more advanced method using characteristics.

4.2.5. Electric field. The application of the electric field is the most complicated part of KALOS. The electric field acts as an advection in momentum space. Because of the spherical co-ordinate system in momentum space, any acceleration involves a partial differential in magnitude of momentum and a mixing in n and m of spherical harmonics. The equations become more straightforward if two differential functions are defined and numerically calculated:

$$G_n^m(p) = p^n \frac{\partial(p^{-n} f_n^m)}{\partial p}; \qquad H_n^m(p) = \frac{1}{p^{n+1}} \frac{\partial(p^{n+1} f_n^m)}{\partial p}. \tag{37}$$

The effect on all m ($m \geqslant 0$) of the electric field in the x direction is then given by

$$\mathcal{E}_{n,x}^m = \frac{eE_x}{m_e} \left[\frac{n-m}{2n-1} G_{n-1}^m + \frac{n+m+1}{2n+3} H_{n+1}^m \right]. \tag{38}$$

For $m > 0$, the combined effect of the electric field in the y and z directions is given by

$$\begin{aligned} \mathcal{E}_{n,y}^m + \mathcal{E}_{n,z}^m = \frac{1}{2} \frac{e}{m_e} \Bigg[& \frac{E_y - \mathrm{i}E_z}{2n-1} G_{n-1}^{m-1} - \frac{E_y + \mathrm{i}E_z}{2n-1} (n-m)(n-m-1) G_{n-1}^{m+1} \\ & - \frac{E_y - \mathrm{i}E_z}{2n+3} H_{n+1}^{m-1} + \frac{E_y + \mathrm{i}E_z}{2n+3} (n+m+1)(n+m+2) H_{n+1}^{m+1} \Bigg] \end{aligned} \tag{39}$$

For $m = 0$,

$$\Re[\mathcal{E}_{n,y}^0 + \mathcal{E}_{n,z}^0] = \Re\left[\frac{e}{m_e} (E_y + \mathrm{i}E_z) \left[-\frac{n(n-1)}{2n-1} G_{n-1}^1 + \frac{(n+1)(n+2)}{2n+3} H_{n+1}^1 \right] \right].$$

Solution by 2nd order Runge–Kutta, as used in spatial advection, gives good results and has the advantage of simplicity. In the first momentum cell close to $p = 0$, the differentials G_n^m and H_n^m are calculated using the assumption that $f_n^m(p) = f_n^m(\Delta p)(p/\Delta p)^n$ if $n > 0$ and that $f_0^0(p) = f_0^0(0) + (f_0^0(\Delta p) - f_0^0(0))(p/\Delta p)^2$, where $p = \Delta p$ is the first grid-point away from the origin at which f_n^m is known. Usually only f_0^0, f_1^0 and f_1^1, and optionally f_2^0, f_2^1 and f_2^2, are allowed to be non-zero in the first cell. Higher order spherical harmonics would give an angular resolution exceeding the resolution in magnitude of momentum p. This is of no advantage and limits the timestep unduly.

Alternatively, the electric field equations naturally fit a leap-frog scheme in which f_n^m at even and odd n leap-frog over each other in time and momentum. This scheme was used initially [1] and works very well for problems in which the momentum calculation dominates, but it introduces momentum averaging in the spatial calculation.

The electric field itself is updated in time from the Maxwell equation $\partial \boldsymbol{E}/\partial t = c^2 \nabla \wedge \boldsymbol{B} - \boldsymbol{j}/\epsilon_0$. This equation can be solved implicitly with an arbitrary timestep, Δt. If solved explicitly, the timestep must be shorter than ω_p^{-1}, or else $\boldsymbol{j}$ must be multiplied by a suitably small factor to make the effective ω_p^{-1} larger than the desired timestep. The magnetic field is straightforwardly calculated from $\partial \boldsymbol{B}/\partial t = -\nabla \wedge \boldsymbol{E}$ provided the numerical scheme maintains $\nabla \cdot \boldsymbol{B} = 0$.

4.3. KALOS: further extensions and applications

The equations outlined above lie at the heart of KALOS. One of the strengths of a finite difference code over a particle code is that it provides a solid platform for the inclusion of further physics. Atomic physics is an important part of laser-produced plasma experiments. It is central to many diagnostics, and ionization determines the number of free electrons, their

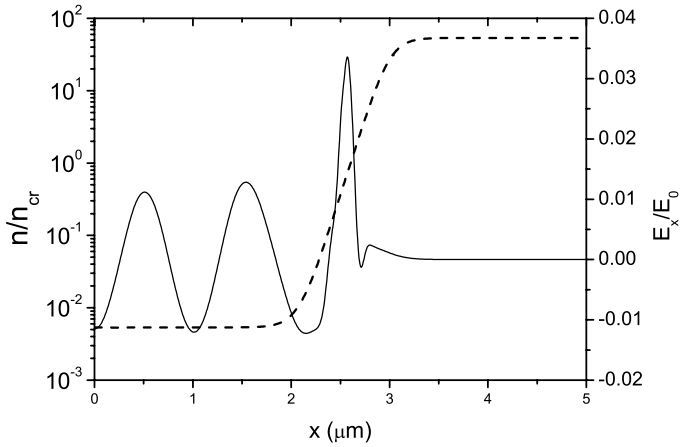

Figure 1. Resonance absorption; plot of electron density (- - - -) and electric field normal to the target (——).

collisionality (through the ion charge Ze) and the resistivity. The fast electrons generated at the start of the laser pulse propagate into an un-ionized plasma with no free electrons. Robinson *et al* [2] have included ionization into KALOS and demonstrated the development of a fast electron front in which both field and collisional ionization are important. Fast electrons cannot penetrate ahead of the front because of the lack of free electrons to carry a return current. KALOS has proved able to resolve the electron distribution on the scale of the ionization energy while simultaneously modelling the propagation of fast electrons with energies of many kiloelectronvolts.

At high intensities with short laser pulses, absorption and transport are coupled problems. Absorption produces the fast electrons which are transported, and transport determines the state of the plasma into which the laser energy is absorbed since fast electron density can exceed the critical density. Absorption, being collisionless at high intensity, has traditionally been modelled with a PIC code, while transport, since it involves collisions, has traditionally been modelled with VFP codes. KALOS offers the possibility of modelling both processes self-consistently with the same code, and initial coupled calculations have been made by Sherlock *et al* [3]. Figure 1 is a graph of a simulation of resonance absorption in a collisional plasma ($Z = 13$) with a sharp density gradient (scalelength $= 0.2$ laser wavelengths). The laser intensity is $10^{14}\,\mathrm{W\,cm^{-2}}$ and the laser is incident on the plasma at a small oblique angle of $\pi/32$. Oblique incidence is modelled in one spatial dimension using a velocity boost similar to that used in [42]. The figure plots the component of the electric field normal to the target surface in units of $\lambda_{\mathrm{Debye}}\omega_{\mathrm{p}}^2 m_{\mathrm{e}}/e$, and the electron density is given relative to the critical density. The initial electron temperature is 50 eV, which gives $v_{\mathrm{osc}}/v_{\mathrm{thermal}}$ (ratio of oscillation velocity in the vacuum laser field to the electron thermal velocity) equal to 1.6. A temperature of 50 eV is much lower than that usually accessible with a PIC code. These results demonstrate the potential of KALOS for modelling combined absorption and transport in a collisional plasma.

The plasma/vacuum interface at the rear of the target is also important because ion acceleration occurs in the electric field sheath caused by fast electrons passing into the vacuum [61–63]. Many aspects of this can be treated one-dimensionally with a traditional collisionless Vlasov code [2], but collisions and ionization in the plasma surface determine the supply of ions into the sheath and this requires a code such as KALOS.

At present, ion motion has not been included in KALOS, but the first stage would be to treat the ions as a fluid and define the electron distribution in the local ion rest frame.

KALOS has the potential for application to many different types of plasmas. The expansion in spherical harmonics makes it particularly suitable for transport dominated by magnetic field since the rotation of electron trajectories is represented by algebraic expressions and does not involve differentials in momentum space. KALOS is particularly suitable for magnetized particle transport when the distribution is nearly isotropic because only a small number of spherical harmonics is needed and, unlike particle codes, it does not need to spend a large amount of computer time modelling the isotropic part of the distribution. Thus, KALOS may be useful for magnetic confinement fusion and for space and astrophysical plasmas where magnetic field dominates.

5. Conclusion

Fast electron transport at high laser intensities around 10^{18} W cm^{-2} is very different from that at intensities closer to the ICF regime. Fast electron penetration into the target is dominated by electric and magnetic fields. Although the fast electrons themselves are essentially collisionless, collisions play a large part in their transport through the all-important return current of thermal electrons which must locally be nearly opposite to the fast electron current. The electric field is able to inhibit fast electron penetration, and the magnetic field is able to collimate the fast electrons into a tight beam. The basic difficulty in simulation is the need to encompass both collisionless fast electrons and highly collisional thermal electrons in the same self-consistent simulation. Hybrid codes separate the two distributions, but run-away effects, non-Maxwellian distortion of the thermal distribution and promotion of thermal electrons into fast electrons in the absorption region mean that for some problems the electron populations cannot be separated and a unified treatment is needed as provided by KALOS.

References

[1] Bell A R and Kingham R J 2003 *Phys. Rev. Lett.* **88** 045004
[2] Robinson A P L *et al* 2005 *Proc. 32nd EPS Conf. on Plasma Physics (Tarragona, Spain, 2005)*
[3] Sherlock M, Bell A R and Rozmus W 2005 *Proc. 32nd EPS Conf. on Plasma Physics (Tarragona, Spain, 2005)*
[4] Davies J R 2003 *Phys. Rev.* E **68** 056404
[5] Malone R C, McCrory R L and Morse R L 1975 *Phys. Rev. Lett.* **34** 721
[6] Bell A R, Evans R G and Nicholas D J 1981 *Phys. Rev. Lett.* **46** 243
[7] Bell A R 1995 *Proc. 45th Scottish Summer Universities Summer School on Inertial Confinement Fusion (St Andrews, UK)* ed M B Hooper
[8] Brunel F 1987 *Phys. Rev. Lett.* **59** 52
[9] Gibbon P 1994 *Phys. Rev. Lett.* **73** 664
[10] Beg F N *et al* 1997 *Phys. Plasmas* **4** 447
[11] Huba J D 1994 *NRL Plasma Formulary* (Washington DC: Naval Research Laboratory)
[12] Milchberg H M, Freeman R R, Davey S C and More R M 1988 *Phys. Rev. Lett.* **61** 2364
[13] Bernardinello A *et al* 2001 *Laser Part. Beams* **19** 59
[14] Pisani F *et al* 2000 *Phys. Rev.* E **62** 5927
[15] Pretzler G, Schlegel T and Fill E 2001 *Lasers Part. Beams* **19** 91
[16] Feurer T *et al* 1997 *Phys. Rev.* E **56** 4608
[17] Bell A R *et al* 1997 *Plasma Phys. Control. Fusion* **39** 653
[18] Guerin S M *et al* 1999 *Plasma Phys. Control. Fusion* **41** 285
[19] Wesson J 2004 *Tokamaks* (Oxford: Clarendon)
[20] Bell A R, Davies J R and Guerin S M 1998 *Phys. Rev.* E **58** 2471
[21] Glinsky M E 1995 *Phys. Plasmas* **2** 2796
[22] Tatarakis M *et al* 2002 *Nature* **415** 280

[23] Wagner U *et al* 2004 *Phys. Rev.* E **70** 026401
[24] Sandhu A S *et al* 2002 *Phys. Rev. Lett.* **89** 225002
[25] Haines M G 2001 *Phys. Rev. Lett.* **87** 135005
[26] Haines M G 1997 *Phys. Rev. Lett.* **78** 254
[27] Weibel E S 1959 *Phys. Rev. Lett.* **2** 83
[28] Romanov D V, Bychenkov V Yu, Rozmus W, Capjack C E and Fedosejevs R 2004 *Phys. Rev. Lett.* **92** 215004
[29] Epperlein E M 1985 *Plasma Phys. Control. Fusion* **27** 1027
[30] Epperlein E M and Bell A R 1987 *Plasma Phys. Control. Fusion* **29** 85
[31] Tatarakis M *et al* 1998 *Phys. Rev. Lett.* **81** 999
[32] Gremillet L *et al* 1999 *Phys. Rev. Lett.* **83** 5015
[33] Borghesi *et al* 1999 *Phys. Rev. Lett.* **83** 4309
[34] Koch J A *et al* 2002 *Phys. Rev.* E **65** 016410
[35] Li Y T *et al* 2001 *Phys. Rev.* E **64** 046407
[36] Davies J R, Bell A R and Tatarakis M 1999 *Phys. Rev.* E **59** 6032
[37] Honrubia J J, Antonicci A and Moreno D 2004 *Laser Part. Beams* **22** 129
[38] Gremillet L, Bonnaud G and Amiranoff F 2002 *Phys. Plasmas* **9** 941
[39] Honda M 2004 *Phys. Rev.* E **69** 016401
[40] Fuchs J *et al* 2003 *Phys. Rev. Lett.* **91** 225002
[41] Stephens R B *et al* 2004 *Phys. Rev.* E **69** 066414
[42] Gibbon P and Bell A R 1992 *Phys. Rev. Lett.* **68** 1535
[43] Wilks S C, Kruer W L Tabak M and Langdon A B 1992 *Phys. Rev. Lett.* **69** 1383
[44] Town R P J, Bell A R and Rose S J 1995 *Phys. Rev. Lett.* **74** 924
[45] Ethier S and Matte J-P 2001 *Phys. Plasmas* **8** 1650
[46] Epperlein E M, Rickard G J and Bell A R 1988a *Comput. Phys. Commun.* **52** 7
[47] Epperlein E M, Rickard G J and Bell A R 1988b *Phys. Rev. Lett.* **61** 2453
[48] Rickard G J, Epperlein E M and Bell A R 1989 *Phys. Rev. Lett.* **62** 2687
[49] Albright B J, Winske D, Lemons D S, Daughton W and Jones M E 2003 *IEEE Trans. Plasma Sci.* **31** 19
[50] Eliasson B 2003 *J. Comput. Phys.* **190** 501
[51] Matte J P and Virmont J 1982 *Phys. Rev. Lett.* **49** 1936
[52] Kingham R J and Bell A R 2002 *Phys. Rev. Lett.* **88** 045004
[53] Kingham R J and Bell A R 2004 *J. Comput. Phys.* **194** 1
[54] Alouani-Bibi F, Shoucri M M and Matte J-P 2004 *Comput. Phys. Commun.* **164** 60
[55] Matte J P *et al* 1988 *Plasma Phys. Control. Fusion* **30** 1665
[56] Davies J R 2002 *Phys. Rev.* E **65** 026407
[57] Welch D R, Rose D V, Oliver B V and Clark R E 2001 *Nucl. Instrum. Methods Phys. Res.* A **464** 134
[58] Gibbon P, Beg F N, Clark E L, Evans R G and Zepf M 2004 *Phys. Plasmas* **11** 4032
[59] Shkarofsky I P, Johnston T W and Bachynski M P 1966 *The Particle Kinetics of Plasmas* (Reading, MA: Addison-Wesley)
[60] Chang J S and Cooper G 1970 *J. Comput. Phys.* **6** 1
[61] Cowan T E *et al* 2004 *Phys. Rev. Lett.* **92** 204801
[62] Mora P 2003 *Phys. Rev. Lett.* **90** 185002
[63] Robinson A P L *et al* 2006 *Phys. Rev. Lett.* **96** 035005